SEISMIC PERFORMANCE OF DIAPHRAGMS IN SLAB-ON-GIRDER STEEL BRIDGES

Seyed M ZAHRAI[1] And Michel BRUNEAU[2]

SUMMARY

Ductile end-diaphragms have been recently proposed as a seismic retrofit strategy to protect the substructures of existing steel slab-on-girder bridges from damage during earthquakes. This paper presents the results from an experimental work to investigate the adequacy of some proposed details. Cyclic tests on full size girder specimens having the proposed ductile diaphragms demonstrate their adequate initial elastic stiffness, strength and capacity to dissipate hysteretic energy in the intended manner. The specimens developed a rotational capacity of 0.2 rad when Triangular plates Added Damping And Stiffness (TADAS) energy dissipation devices were used, and link distortion angles of 0.08 to 0.11 rad when Eccentrically Braced Frame (EBF) and Shear Panel Systems (SPS) were in place, corresponding to average ductilities of 8 to 10 before failure. However, specimens without any diaphragm dissipated significantly less hysteretic energy, and suffered buckling of the web stiffeners and fracture of the stiffeners welds at large drifts.

INTRODUCTION

Damage to abutments, piers, bearings, foundations, and other substructure elements of existing bridges during recent earthquakes (e.g. Northridge and Kobe) has proven to be catastrophic, often leading to span collapses (Astaneh-Asl et al. 1994; Bruneau et al. 1996). Earlier research has demonstrated how substructure damage in slab-on-girder steel bridges can be prevented if the existing end-diaphragms over abutments and piers are replaced with specially designed ductile diaphragms calibrated to yield before the strength of the substructure is reached (Zahrai and Bruneau 1999a). Interior diaphragms need not be replaced as they do not contribute to the lateral load resistance (Zahrai and Bruneau 1998). This alternative seismic retrofit strategy has been analytically validated for bridges supported on stiff substructures, and shown to be inappropriate in the presence of flexible substructures. Although its success relies on energy dissipating devices previously used in building applications, experimental work is needed to prove their effectiveness and establish appropriate details within the proposed ductile bridge diaphragms.

To that end, a series of cyclic tests were carried out on full-scale specimens, each having a ductile end-diaphragm introduced between two short segments of main girders. The results of this experimental work are reported in this paper, along with practical recommendations.

EXPERIMENTAL APPROACH

[1] *Assistant Professor, Dept. od Civil Engineering, Univ. of Tehran, P.O. Box 11365-4563, Tehran, Iran; Fax 98-21-661024*
[2] *Professor, Dept. of Civil, Struc. & Env. Engrg, State Univ. of New York at Buffalo, 130 Ketter Hall, Buffalo, New York*

Design of Test Specimens

Prior research (Zahrai and Bruneau 1998) on the lateral load resistance and deflected shape of steel slab-on-girder bridges has demonstrated that only the end-diaphragms and the girder segments having bearing stiffeners and located near the supports effectively contribute to the total lateral load resistance (unless numerous tightly spaced intermediate web stiffeners are present). For that reason, a short girder segment that includes the diaphragm and bearing stiffeners can effectively capture the lateral response behavior of slab-on-girder bridges. Specimens considered here were designed accordingly, assuming one ductile diaphragm at each bridge end.

As such, specimens representative of existing 40 m span steel slab-on-girder bridges were achieved by using two 0.5 m long segments of WWF1200x333 girders, 2 m center-to-center, and having 10 mm thick and 100 mm wide bearing web stiffeners on each side of the web. A 200 mm thick reinforcement concrete deck, connected to the top flange of each girder segment by 10 shear studs, was poured in place during construction of the specimens. These girders were then joined by the same three types of ductile end-diaphragm systems considered in the prior analytical study (Zahrai and Bruneau 1999a), i.e. TADAS, EBF and SPS. All three shared a chevron braced frame configuration, with a bottom beam, and two double angles as diagonal braces. The systems were sized following the retrofit design procedure presented elsewhere (Zahrai and Bruneau 1999a), considering that the entire bridge (with 4 girders) should be able to resist a design peak ground acceleration of approximately 0.5g.

Following the proposed design procedure (Zahrai and Bruneau 1999a), the TADAS device was designed with four 25 mm thick triangular plates having height and base width of 105 and 80 mm respectively, and providing a device stiffness and strength of 150 kN/mm and 167 kN respectively. The base of the TADAS plate assembly was bolted to the bottom beam. The EBF link length was chosen to be 300 mm, providing a shear yield capacity of 124 kN, which translated into a diaphragm shear strength of 235 kN. Two different SPS designs were considered. First, a W200x15 shear link (SPS1) welded directly to the top flange of the bottom beam was considered. Second, a 175 mm long link section (SPS2) was built-up using two 130x45x8 [mm] plates for each flange, a 175x130x5 web plate, and one 148x45x6 horizontal stiffener on each side at mid-height, and welded to a 280x120x10 base plate bolted to the top flange of the bottom beam using 8 M20 bolts. Other sizes and details of the surrounding structural elements are illustrated in subsequent figures. Braces, bottom beams (outside of the links) and all connections were designed to remain elastic.

CAN/CSA G40.21-M 350W structural steel (equivalent to ASTM-A572 Grade 50) was specified for all steel specimens. Nominal yield and tensile strengths of 350 and 450 MPa, respectively, were used in designing test specimens. Coupon tests revealed yield strengths of 10 to 20% higher than the nominal values.

Test set-up

All specimens were subjected to progressively increasing cyclic lateral displacement following as much as possible the ATC-24 protocol (Applied 1992). A constant gravity load of 350 kN (i.e. 175 kN per girder), equal to half of the value that would result by integrating the shear stresses along the web of the girders, was applied to the specimens deck slabs using two vertical actuators. This equivalent load was selected because it created the same P-Δ effects on the specimens and actual bridge. All specimens were instrumented for displacement and strain measurements at the points of interest, and were whitewashed to help observe the yielding patterns and their progression. Refer to (Zahrai and Bruneau 1999b) for details on design of the specimens or their instrumentation.

Experiment on TADAS End-Diaphragm

The TADAS specimen, shown in Figure 1a, was subjected to 21 cycles of lateral loading before failure occurred at 4% drift. The final lateral load-deflection curves for the specimen are shown in Figure 1b. Note that the hysteretic loops experienced pinching due to connection slippage and existing gaps ranging from 1 to 2 mm between the top of each TADAS plate and their reaction points, at the early stage of loading (these gaps were introduced by the fabricator even though the drawings called for a perfect fit).

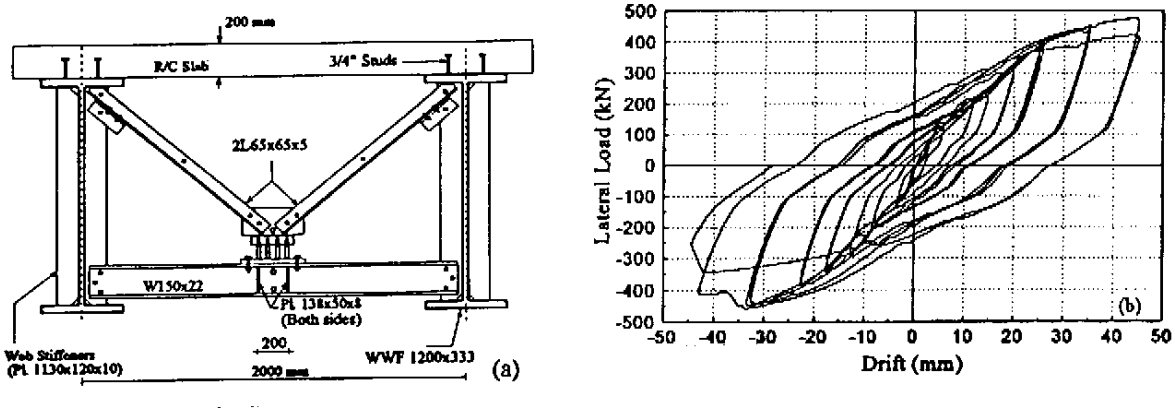

Figure 1. Ductile end-diaphragm specimen having TADAS: (a) elevation; (b) hysteretic curves

Strain gage data showed that some TADAS plates started to yield at drifts of approximately 1% (variable gap sizes prevented simultaneous yielding), with all TADAS plates yielding when drifts reached 20 and -18 mm (1.5% drift), corresponding to lateral loads of 320 and -350 kN. Fine cracks were observed in the whitewash paint near the top of the TADAS plates.

As shown in Figure 2, the TADAS plates bent noticeably during the three cycles at displacements of 25 and -23 mm (2% drift). At that time, the paint on the surface of TADAS plates showed evidence of extensive yielding. The experiment ended after flexural failure of three TADAS plates and local buckling of the girder web stiffeners at 4% drift.

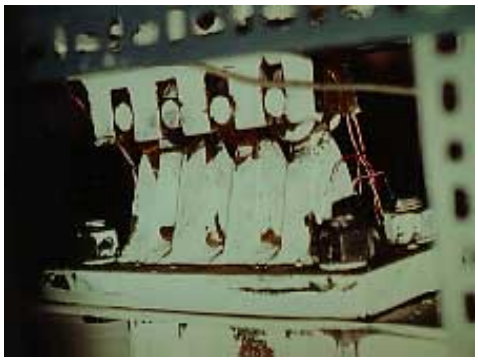

Figure 2. TADAS plates under huge flexure at 2% drift

Experiment on EBF End-Diaphragm

The EBF end-diaphragm tested is shown in Figure 3a. As the specimen was loaded up to a 3% drift, a great deal of slip was observed in all bolted connections. Figure 3b shows the highly pinched hysteretic curves obtained in the 24 cycles applied to this specimen in the first phase of its testing. Since this extensive slippage was detrimental to the intended ductile performance of the system as larger drifts were required to fully develop yielding within the ductile eccentric link, testing was stopped prior to failure of the ductile link or buckling of the girder web stiffeners, and the specimen was re-tested after welding all bolted connections.

Figure 3. Ductile end-diaphragm specimen having EBF: (a) elevation; (b) hysteretic curves (bolted EBF); (c) shear distortion and local buckling at the link; (d) hysteretic curves (welded EBF)

Symmetric and full hysteretic curves were obtained for this all-welded EBF ductile diaphragm as no slippage occurred contrary to the previous diaphragm test. Yielding of the EBF started at drifts of roughly 5 mm. Large shear distortions of the link became progressively more visible during cycles at 2δy and 3δy drift (1% drift). Some strength degradation was observed on the hysteretic curves during cycles at 6δy (2% drift) as the north side of the east end of the link developed significant visible local buckling (Figure 3c) causing a slight drop in shear resistance. Sideway deflection at the west end of the link increased to 2.8 mm and severe flange distortion ensued. When the specimen was subjected to its 22nd cycle, the first at a displacement of 30 mm (8δy , or 2.5% drift), the link beam failed due to sudden lateral displacement of the link. As a result of this instability, brittle fracture occurred at the west end of the link flange and buckling developed at the east end of the same flange. Figure 3d shows the hysteretic loops for this experiment which reached maximum lateral loads of 640 and -650 kN. This failure might have been prevented or delayed had the ends of the link beam been laterally braced (although this was deliberately not done in this case because the short length and lateral stiffness of the bottom beam suggested that this EBF link could reach its target plastic shear distortion of 0.10 rad prior to instability (and it did), lateral bracing is a mandatory requirement for EBFs).

Experiment on SPS End-Diaphragm

The SPS specimen (Figure 4a) was subjected to 28 cycles of lateral loading until failure occurred at a 3% drift. The resulting hysteretic curves (Figure 4b) show good energy dissipation and less pinching compared to those of TADAS and bolted EBF.

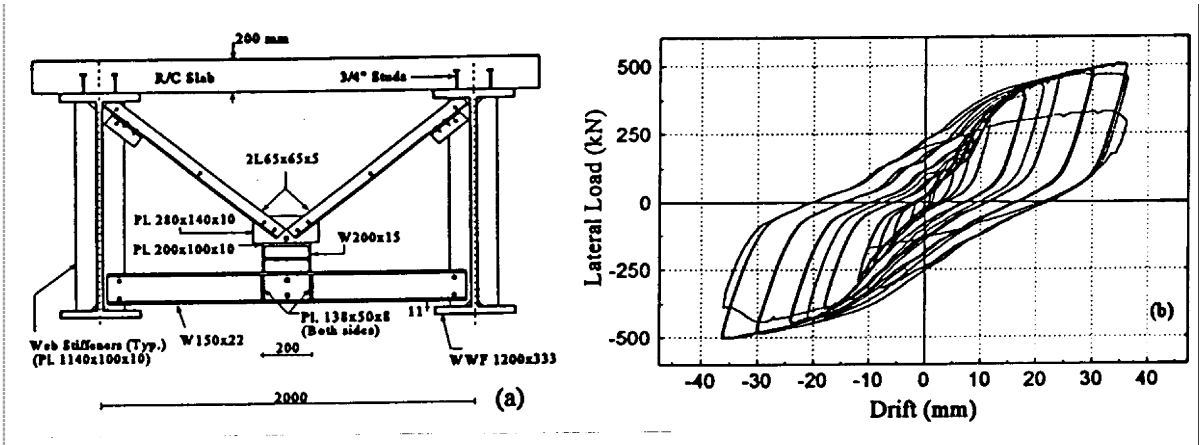

Figure 4. Ductile end-diaphragm specimen having SPS: (a) elevation; (b) hysteretic curves

Strain gages showed that yielding of the shear panel started at drifts of ±9 mm. Fine cracks formed in the whitewash on web of the shear panel during the cycles at ±12 mm (1% drift) corresponding to lateral forces of 320 and -300 kN, and the hysteretic load-deflection curves started to exhibit evidence of large plastification. Measured panel rotation (almost equal to shear distortion) was about 0.02, while the strains read by the rosettes on SPS web reached 8000 με. At large lateral drifts of ±18 mm (1.5% drift), the shear panel visibly deformed as

a parallelogram bounded by the end plates and flanges (Figure 5). Localized severe distortions started to form in the vertical shear panel.

Figure 5. Deformation of the vertical link (SPS) as a parallelogram link and visible buckling in the flanges

The SPS flanges started to buckle visibly during the cycles at ±30 mm (2.5% drift) corresponding to lateral loading of 480 kN. However, hysteretic curves were still stable with no strength degradation. Finally during cycles at ±36 mm (3% drift), severe local buckling developed in the flanges at the lower end of the shear panel. The base of the link fractured at one flange during the third of these cycles, with a crack propagating through the link during an additional cycle at the same drift. Note that, although not recommended, this SPS device was not laterally braced; however, its lateral deflection did not exceed 1.5 mm.

HYSTERETIC RESPONSE OF DUCTILE DEVICES

Lateral load versus drift hysteretic curves presented above attest to the good energy dissipation of the ductile diaphragms considered here, although bolted diaphragms did not perform as well as those welded due to bolt slippage. For the TADAS specimen, a maximum curvature of 1.2 rad/m was achieved leading to a curvature ductility of 8 for the TADAS device. The hysteretic curves for the EBF specimens showed that the link beam started to yield in flexure (in addition to their dominant shear yielding) during the last cycles of testing, and that curvature ductilities of approximately 6 and 8.5 were obtained at the shear link ends in the bolted and welded EBFs. For the bottom of the vertical link in the SPS specimen, yielding initiated at curvature of about 0.025 rad/m, corresponding to an average maximum curvature of 0.25 rad/m, reflecting a curvature ductility of about 8, demonstrating that the shear panels experienced significant flexural yielding in addition to their primary shear yielding.

Yield and maximum distortion angles of 0.075 and 0.29 rad, respectively, gave a ductility of 6 for the TADAS device. These experimental results were in agreement with the TADAS distortion ductility capacity of at least 0.25 rad reported previously (Tsai et al. 1993). Corresponding values of 0.007 and 0.055 rad for the bolted EBF specimen (with a distortion angle of 0.007 rad due to slippage), and 0.008 and 0.11 rad for the welded EBF specimen, respectively, gave link rotational ductilities of 8 and 14. The SPS device yielded at link rotation of 0.009 rad (after deducting 0.003 rad due to the measured slippage), corresponding to a shear force of 185 kN, reaching a link rotational ductility of 13.

Experiment on Specimen without Diaphragm

After dismantling all the end-diaphragm members, the remaining specimen with the two stiffened girders alone was tested to failure. The web stiffeners had cracks propagating from the bolt holes where diaphragm were connected before to the free edge of the stiffeners. In spite of this damage, 25 cycles up to a maximum drift of ±96 mm (8%) were applied to the specimen. Figure 6 shows the lateral load versus drift hysteretic curves for this specimen. Testing stopped after the specimen experienced severe buckling of the web stiffeners, fracture of full penetration welds at the top and bottom of the girder bearing stiffeners.

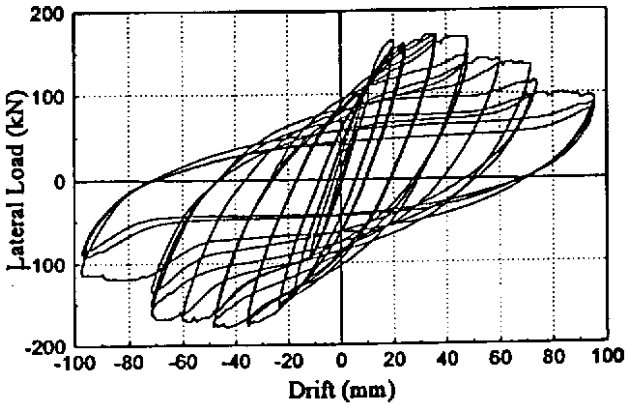

Figure 6. Hysteretic curves for the specimen without diaphragm

ENERGY DISSIPATION

To provide a better comparison of the hysteretic energies dissipated by the various specimens, these energies per cycle are plotted at given drifts, as shown in Figure 7. The welded EBF specimen dissipated a larger hysteretic energy per cycle up to its failure at about 3% drift, while the TADAS specimen dissipated more hysteretic energy per cycle at near 4% drift. The specimen without diaphragms dissipated significantly less hysteretic energy per cycle, reflecting its relative ineffectiveness compared to those with ductile diaphragms.

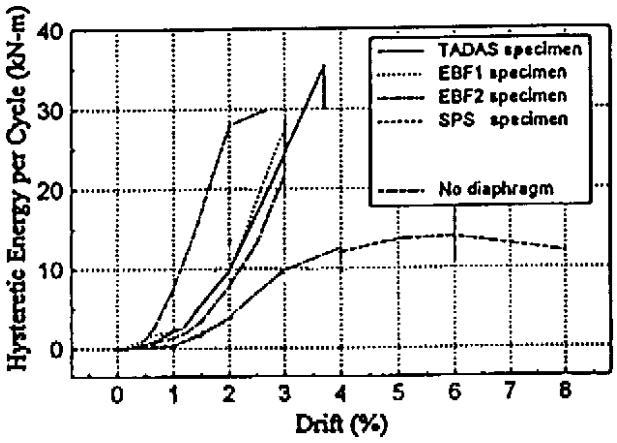

Figure 7. Hysteretic energies per cycle dissipated by the specimens

CONCLUSION

Full scale ductile end-diaphragm specimens designed using the procedure proposed by the authors exhibited adequate strength and capacity to dissipate hysteretic energy, and remained stable up to diaphragm drifts of approximately 3%. Ductile device rotational capacity of 0.2 rad (TADAS) and link distortion angles of 0.08 to 0.11 rad (EBF and SPS), corresponding to average ductilities of 8 to 10, were achieved before failure. Ultimate instability failure of the EBF diaphragm illustrate the importance of providing appropriate lateral supports to the

ductile device. Ductile end-diaphragms having bolted members experienced extensive slippage, leading to pinched hysteretic curves. The welded diaphragm specimen exhibited a significantly improved seismic behavior, dissipating more hysteretic energy at smaller drifts, and closely matched the theoretical expectations. Finally, experiments showed that absence of end-diaphragms may produce excessive drifts and serious damage to the girder web stiffeners.

ACKNOWLEDGMENT

The NSERC of Canada is thanked for its financial support through a Strategic Grant on the Seismic Evaluation of Existing Bridges, and a Collaborative Grant on Innovative Seismic Retrofit of Existing Bridges. The graduate scholarship for the first author by MCHE of Iran is also appreciated. The findings and recommendations in this paper, however, are those of the writers, and not necessarily those of the sponsors.

REFERENCES

Applied Technology Council (1992). *Guidelines for cyclic seismic testing of components of steel structures*. Publication ATC-24, Palo Alto, California.

Astaneh-Asl, A., Bolt, B., Mcmullin, K. M., Donikian, R. R., Modjtahedi, D. and Cho, S. W. (1994), "Seismic performance of steel bridges during the 1994 Northridge earthquake", *UCB report* CE-STEEL 94/01, Berkeley, California.

Bruneau, M., Wilson, J. W. and Tremblay, R. (1996). "Performance of steel bridges during the 1995 Hyogoken-Nanbu (Kobe, Japan) earthquake.", *Canadian J. Civ. Engrg*., 23 (3).

Tsai, K.C., Chen, H.W., Hong, C.P. and Su, Y.F. (1993), "Design of steel triangular plate energy absorbers for seismic-resistant construction", EERI, Earthquake Spectra, (9), No.3, 505-528.

Zahrai, S.M., Bruneau, M. (1998). "Impact of Diaphragms on Seismic Response of Straight Slab-on-girder Steel Bridges", *ASCE Structural Journal*, Vol.124, No.8, pp.938-947.

Zahrai, S. M. and Bruneau, M. (1999a), "Ductile end-diaphragms for seismic retrofit of slab- on-girder steel bridges", *ASCE Structural journal*, Vol.125, No.1, pp.71-80.

Zahrai, S. M. and Bruneau, M. (1999b), "Cyclic testing of ductile end diaphragms for slab-on-girder steel bridges", *ASCE Structural Journal*, Vol.125, No. 9, in press.